ULTRASOUND NEWS

July 2024

Diagnostic performance of quantitative ultrasonography for hepatic steatosis in a health screening program: a prospective single-center study

Jeung Hui Pyo[1*], Soo Jin Cho[1*], Sung Chul Choi[1], Jae Hwan Jee[1], Jeeyeong Yun[1], Jeong Ah Hwang[2], Goeun Park[3], Kyunga Kim[3,4], Wonseok Kang[5,6], Mira Kang[1,4,7], Young Hye Byun[1]

※ Author affiliations appear at the end of this article.

ULTRA SONO GRAPHY

ORIGINAL ARTICLE

https://doi.org/10.14366/usg.24040
eISSN: 2288-5943
Ultrasonography 2024;43:250-262

In conclusion, QUS is an accurate, noninvasive, and widely available diagnostic method that is suitable for detecting and grading hepatic steatosis in asymptomatic patients undergoing health screening. In this study, the combination of QUS and B-mode US achieved the highest AUC. Therefore, the clinical application of QUS in conjunction with conventional B-mode US should be considered for better assessment of hepatic steatosis in health screening programs.

Pyo JH, Cho SJ, Choi SC, et al. Ultrasonography 2024;43:250-262

Diagnostic performance of quantitative ultrasonography for hepatic steatosis in a health screening program: a prospective single-center study

PATIENT

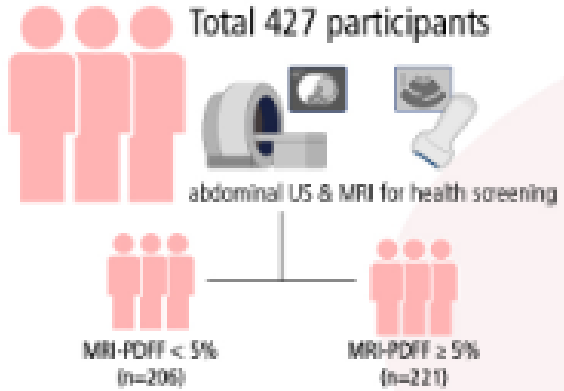

METHOD

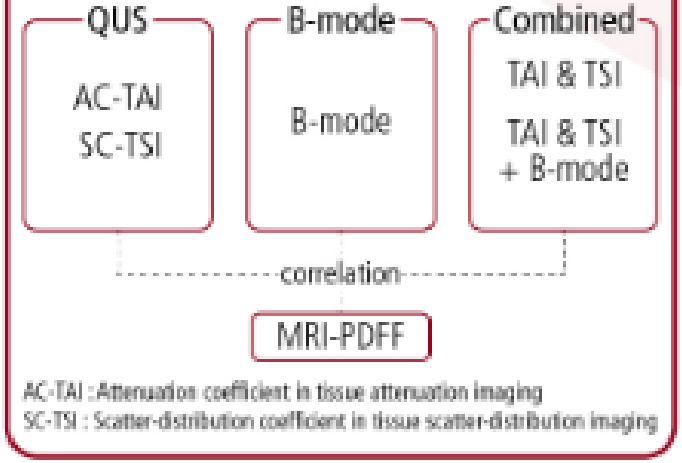

AC-TAI : Attenuation coefficient in tissue attenuation imaging
SC-TSI : Scatter-distribution coefficient in tissue scatter-distribution imaging

RESULT

Hepatic steatosis grade(based on MRI-PDFF)

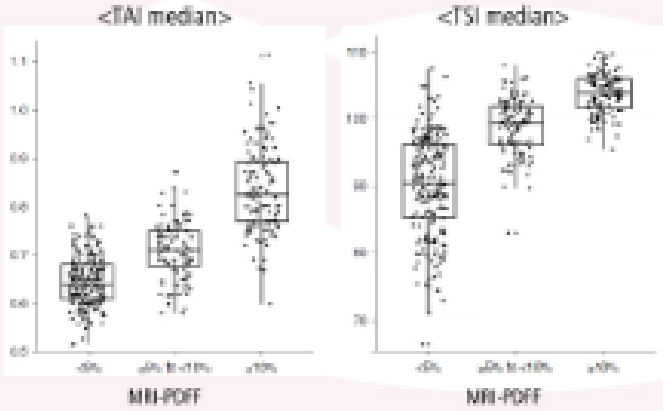

	<5% (n=225)	≥5% to <10% (n=106)	≥10% (n=110)	P-value
TAI	0.64(0.61-0.68)	0.71(0.68-0.75)	0.83(0.77-0.89)	< 0.001
TSI	90.2(82.9-96.1)	99.2(95.9-101.7)	103.7(101.5-105.8)	< 0.001

Diagnostic performance of QUS parameters & visual grade for the detection of hepatic steatosis

	AUC (95% CI)	Cutoff value
MRI-PDFF ≥ 5%		
TAI	0.887(0.857-0.918)	≥ 0.708
TSI	0.910(0.883-0.938)	≥ 98.79
B-mode US	0.878(0.848-0.908)	≥ 1
Combined Model (TAI & TSI)	0.939(0.918-0.959)	≥ 0.513
Combined Model (TAI & TSI + B-mode US)	0.947(0.929-0.966)	≥ 0.426
MRI-PDFF ≥ 10%		
TAI	0.951(0.928-0.973)	≥ 0.748
TSI	0.922(0.897-0.946)	≥ 99.05
B-mode US	0.875(0.848-0.902)	≥ 2
Combined Model (TAI & TSI)	0.972(0.959-0.985)	≥ 0.269
Combined Model (TAI & TSI + B-mode US)	0.975(0.963-0.987)	≥ 0.311

QUS is a useful and effective screening tool for detecting and grading hepatic steatosis during health checkups.

Purpose: This study compared the diagnostic performance of quantitative ultrasonography (QUS) with that of conventional ultrasonography (US) in assessing hepatic steatosis among individuals undergoing health screening using magnetic resonance imaging–derived proton density fat fraction (MRI-PDFF) as the reference standard.

Methods: This single-center prospective study enrolled 427 participants who underwent abdominal MRI and US. Measurements included the attenuation coefficient in tissue attenuation imaging (TAI) and the scatter-distribution coefficient in tissue scatter-distribution imaging (TSI). The correlation between QUS and MRI-PDFF was evaluated. The diagnostic capabilities of QUS, conventional B-mode US, and their combined models for detecting hepatic fat content of ≥5% (MRI-PDFF ≥5%) and ≥10% (MRI-PDFF ≥10%) were compared by analyzing the areas under the receiver operating characteristic curves. Additionally, clinical risk factors influencing the diagnostic performance of QUS were identified using multivariate linear regression analyses.

Results: TAI and TSI were strongly correlated with MRI-PDFF (r=0.759 and r=0.802, respectively; both P<0.001) and demonstrated good diagnostic performance in detecting and grading hepatic steatosis. The combination of QUS and B-mode US resulted in the highest areas under the ROC curve (AUCs) (0.947 and 0.975 for detecting hepatic fat content of ≥5% and ≥10%, respectively; both P<0.05), compared to TAI, TSI, or B-mode US alone (AUCs: 0.887, 0.910, 0.878 for ≥5% and 0.951, 0.922, 0.875 for ≥10%, respectively). The independent determinants of QUS included skin-liver capsule distance (β=7.134), hepatic fibrosis (β=4.808), alanine aminotransferase (β=0.202), triglyceride levels (β=0.027), and diabetes mellitus (β=3.710).

Conclusion: QUS is a useful and effective screening tool for detecting and grading hepatic steatosis during health checkups.

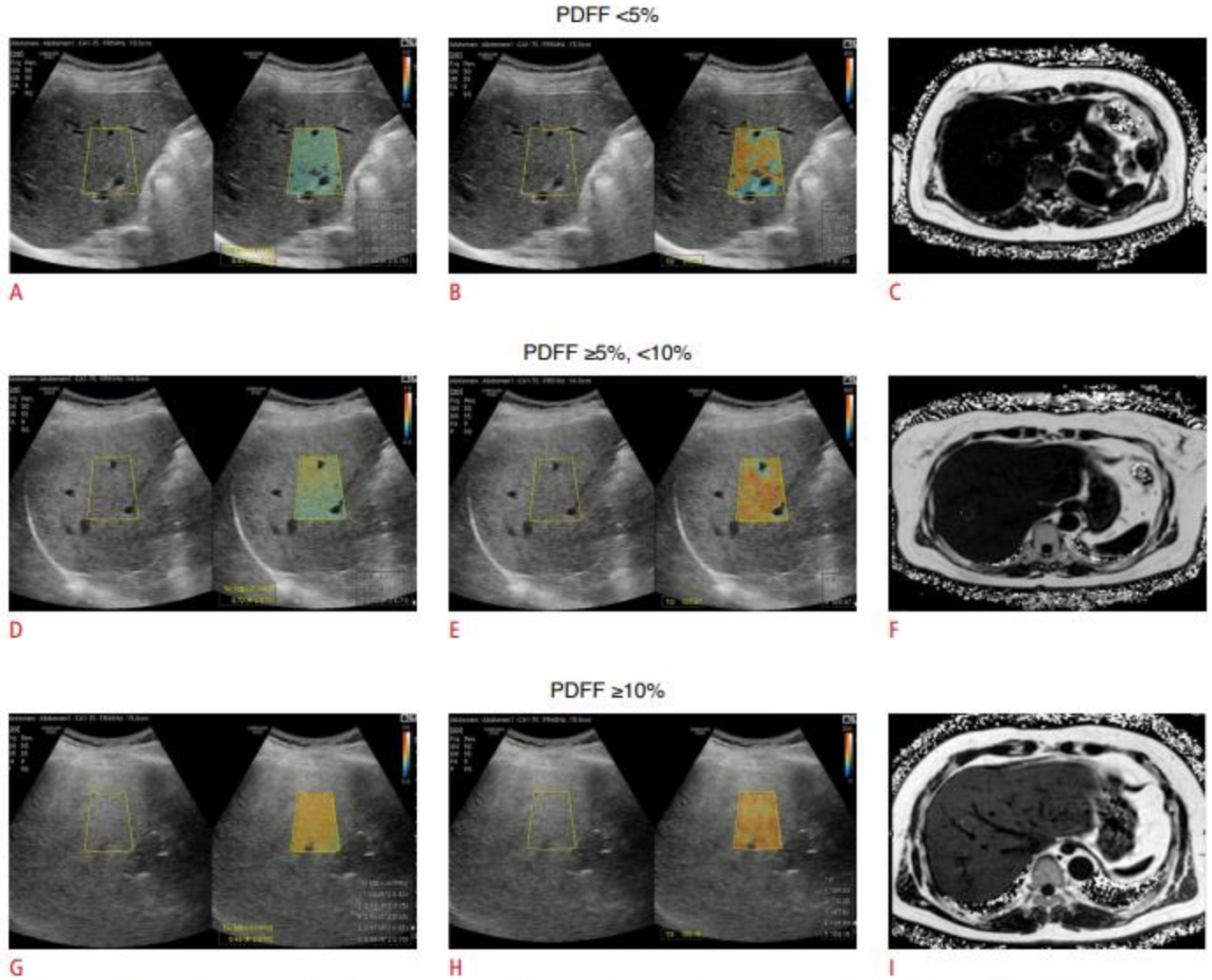

Fig. 2. Quantitative ultrasonographic (US) measurement of liver fat using attenuation coefficient (AC) in tissue attenuation imaging (TAI) and scatter-distribution coefficient (SC) in tissue scatter distribution imaging (TSI).

A–C. In a 54-year-old woman without hepatic steatosis on B-mode US, the AC in TAI (A) and SC in TSI (B) are 0.62 and 81.99, respectively. C. The magnetic resonance imaging–derived proton density fat fraction (MRI-PDFF) measured on the PDFF map as a reference standard is 0.98%. D–F. In a 60-year-old woman with mild hepatic steatosis on B-mode US, the AC in TAI (D) and SC in TSI (E) are 0.72 and 100.67, respectively. F. MRI-PDFF measured on the PDFF map as a reference standard is 8.42%. G–I. In a 56-year-old man with moderate hepatic steatosis on B-mode US, the AC in TAI (G) and SC in TSI (H) are 0.96 and 108.18, respectively. I. MRI-PDFF measured on the PDFF map as a reference standard is 21.06%.

RESEARCH ARTICLE | Open Access

Comparison of lung ultrasound assisted by artificial intelligence to radiology examination in pneumothorax

Chengdi Yang, Huijing Zhao, Anqi Wang, Jian Li, Jianling Gao

First Published: 29 June 2024

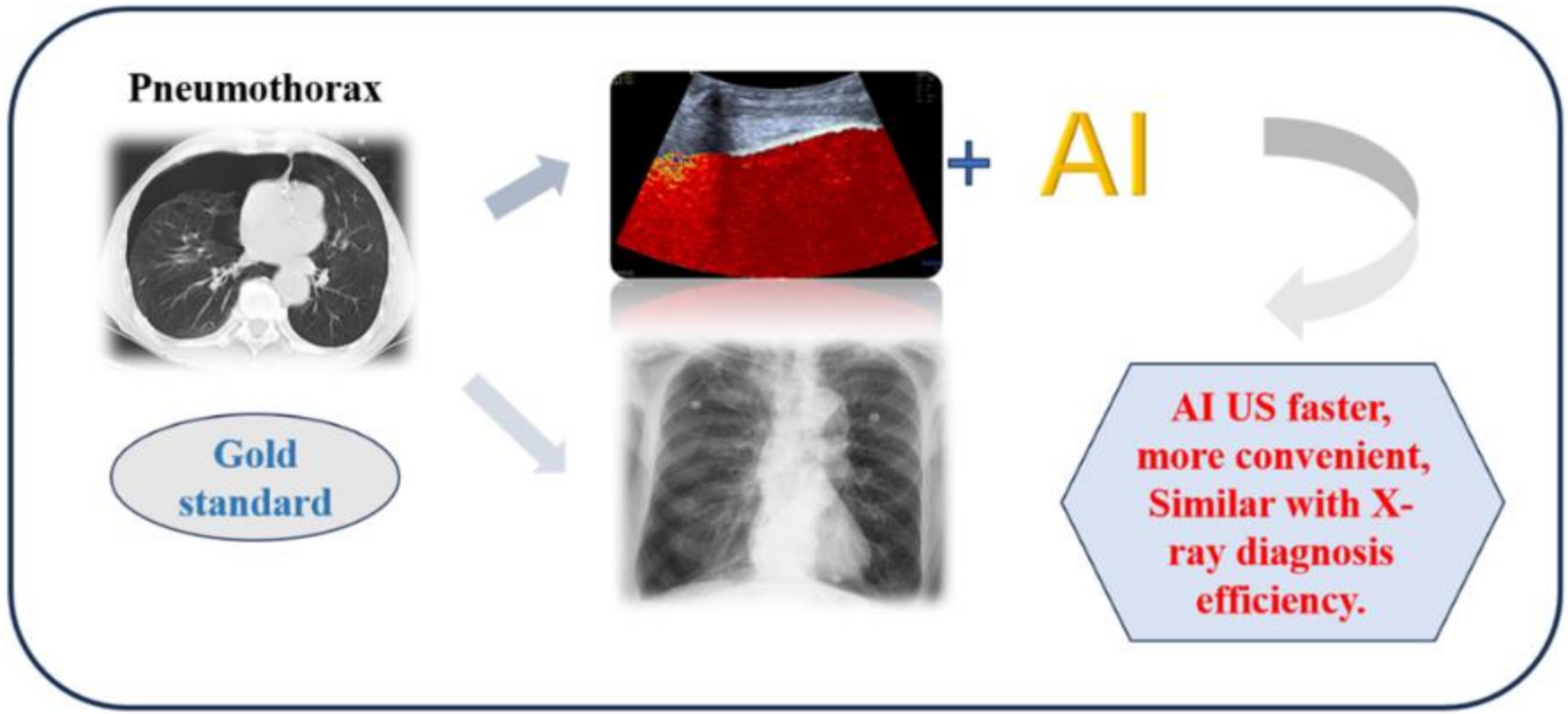

With CT as the gold standard, an artificial intelligence (AI) algorithm was applied to ultrasound. The diagnosis of pneumothorax using AI ultrasound is comparable to x-ray in terms of sensitivity and specificity.

CASE REPORT

Isolated liver gastrointestinal stromal tumor: A case report

Yan Deng, Min Zhang, Shi-Yan Li

First Published: 22 June 2024

Gray scale ultrasound findings of isolated liver gastrointestinal stromal tumor.

Open Journal of Radiology > Vol.14 No.2, June 2024

Check for updates

Quantitative Assessment of Liver Fibrosis by Elastography in Patients with Chronic Liver Disease: A Cross-Sectional Study in Lomé (Togo)

Massaga Dagbe[1*], Bidamin N'timon[1], Sonia Ekembe[2], Rafiou El-Hadji Yakoubou[3], Pihou Gbande[4], Lantam Sonhaye[2], Lama Kegdigoma Agoda-Koussema[2], Komlanvi Victor Adjenou[2]

[1]Department of Radiology and Medical Imaging, Kara University Hospital, Kara, Kara, Togo.

[2]Department of Radiology and Medical Imaging, Lomé University Hospital, Lome, Togo.

[3]Department of Hépato-gastroenterology, Kara University Hospital, Kara, Togo.

[4]Department of Radiology and Medical Imaging, Sokodé Regional Hospital, Sokode, Togo.

[5]Department of Internal Medicine, Kara University Hospital, Kara, Togo.

DOI: 10.4236/ojrad.2024.142005 **PDF** **HTML** **XML** **33** Downloads **123** Views

degree of this hepatic hardness is not related to its **aetiology or to liver enzyme disorders** but, on the contrary, it is related to **hepatic dysmorphia** and increases with the presence of **portal hypertension**. These results underline the fact that the assessment of liver fibrosis in patients with chronic liver disease using this technique is essential for patient follow-up.

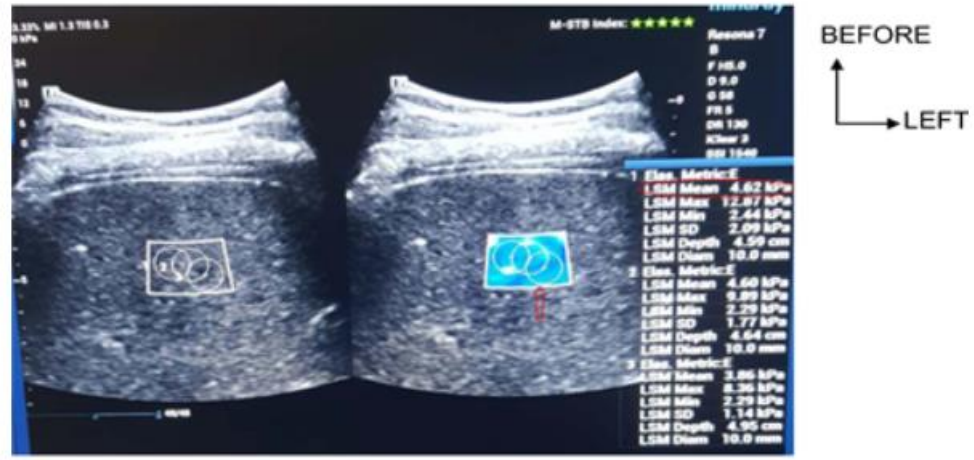

Figure 3. Inter-costal axial section with 2D-SWE measurement of liver elasticity.

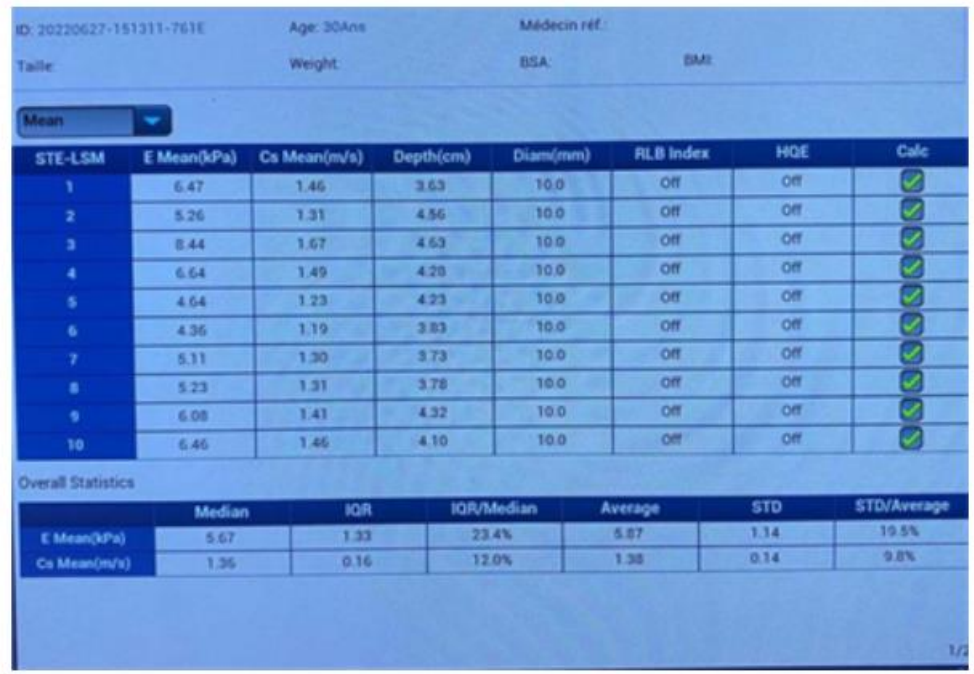

ID: 20220627-151311-761E Age: 30Ans Médecin réf.:

Taille: Weight: BSA: BMI:

Mean

STE-LSM	E Mean(kPa)	Cs Mean(m/s)	Depth(cm)	Diam(mm)	RLB Index	HQE	Calc
1	6.47	1.46	3.63	10.0	Off	Off	✓
2	5.26	1.31	4.56	10.0	Off	Off	✓
3	8.44	1.67	4.63	10.0	Off	Off	✓
4	6.64	1.49	4.28	10.0	Off	Off	✓
5	4.64	1.23	4.23	10.0	Off	Off	✓
6	4.36	1.19	3.83	10.0	Off	Off	✓
7	5.11	1.30	3.73	10.0	Off	Off	✓
8	5.23	1.31	3.78	10.0	Off	Off	✓
9	6.08	1.41	4.32	10.0	Off	Off	✓
10	6.46	1.46	4.10	10.0	Off	Off	✓

Overall Statistics

	Median	IQR	IQR/Median	Average	STD	STD/Average
E Mean(kPa)	5.67	1.33	23.4%	5.87	1.14	19.5%
Cs Mean(m/s)	1.36	0.16	12.0%	1.38	0.14	9.8%

Figure 4. Final report of 2D-SWE liver elasticity measurements.

Abstract

Aim: To describe the two-dimensional elastographic profile according to the Shearwave (2D-SWE) technique in patients with chronic liver disease in Lomé. **Materials and method:** Cross-sectional, descriptive study conducted over seven month at the Autel d'Elie Clinic in Lomé, from January to August 2022, on adult patients with chronic liver disease who underwent abdominal ultrasound coupled with two-dimensional elastography. **Results:** The sample size was 54 patients. The mean age of the patients was 33 ± 12 years, with extremes of 18 and 66 years. Patients aged 30 years or less accounted for 48.1% (n = 26). All patients (n = 54) had at least one transaminase assay with a mean of 69.3 ± 78.3 IU/l (AST) and 59.3 ± 82.8 IU/l (ALT). There was no statistically significant association between the biological parameters and the presence of fibrosis. Viral liver disease was the main cause, accounting for 81.5% (n = 44) of cases, with no significant association with the degree of fibrosis. Ultrasound revealed a dysmorphic liver (57.4%; n = 31) and portal hypertension (18.5%, n = 10). Fibrosis stages F1, F2 and F4 accounted for (48.1%, n = 26), (24.1%, n = 13) and (13%, n = 7) of cases respectively. Liver dysmorphia was significantly associated with the presence of fibrosis (p = 0.012) and portal hypertension was significantly associated with the degree of fibrosis (p = 0.0063). **Conclusion:** Assessment of liver fibrosis in patients with chronic liver disease using 2D-SWE elastography is essential for patient follow-up.

Tuberculosis: A Head to Toe Radiological Review

Alexandre Semionov[1*], Kiana Lebel[2], Ange Diouf[3], Josephine Pressacco[1]

[1]Department of Diagnostic Radiology, McGill University Health Centre, Montreal, Canada
[2]Faculty of Medicine, University of Sherbrooke, Sherbrooke, Canada
[3]Department of Radiology, Radiation Oncology and Nuclear Medicine, Université de Montréal, Montreal, Canada
Email: *alexandre.semionov@mail.mcgill.ca

Abstract

Tuberculosis (TB) results from infection by *Mycobacterium tuberculosis* and can involve any organ or tissue. Early diagnosis of TB is essential for timely initiation of therapy in order to decrease transmission rate and avoid severe morbidity associated with delayed treatment. Although conventional radiography remains the most common initial imaging modality in diagnosis of pulmonary TB, computer tomography (CT) and magnetic resonance imaging (MRI) are modalities of choice with regards to diagnosis of extra-pulmonary TB. The purpose of this paper is to provide a concise review of various imaging manifestations of TB in various organ systems, in order to promote radiologists' and clinicians' familiarity with common radiological findings of this important disease.

Conclusion Tuberculosis is still impacting millions of people worldwide. The intention of this review is to familiarize radiologists and clinicians with common radiologic manifestations of TB in various body systems.

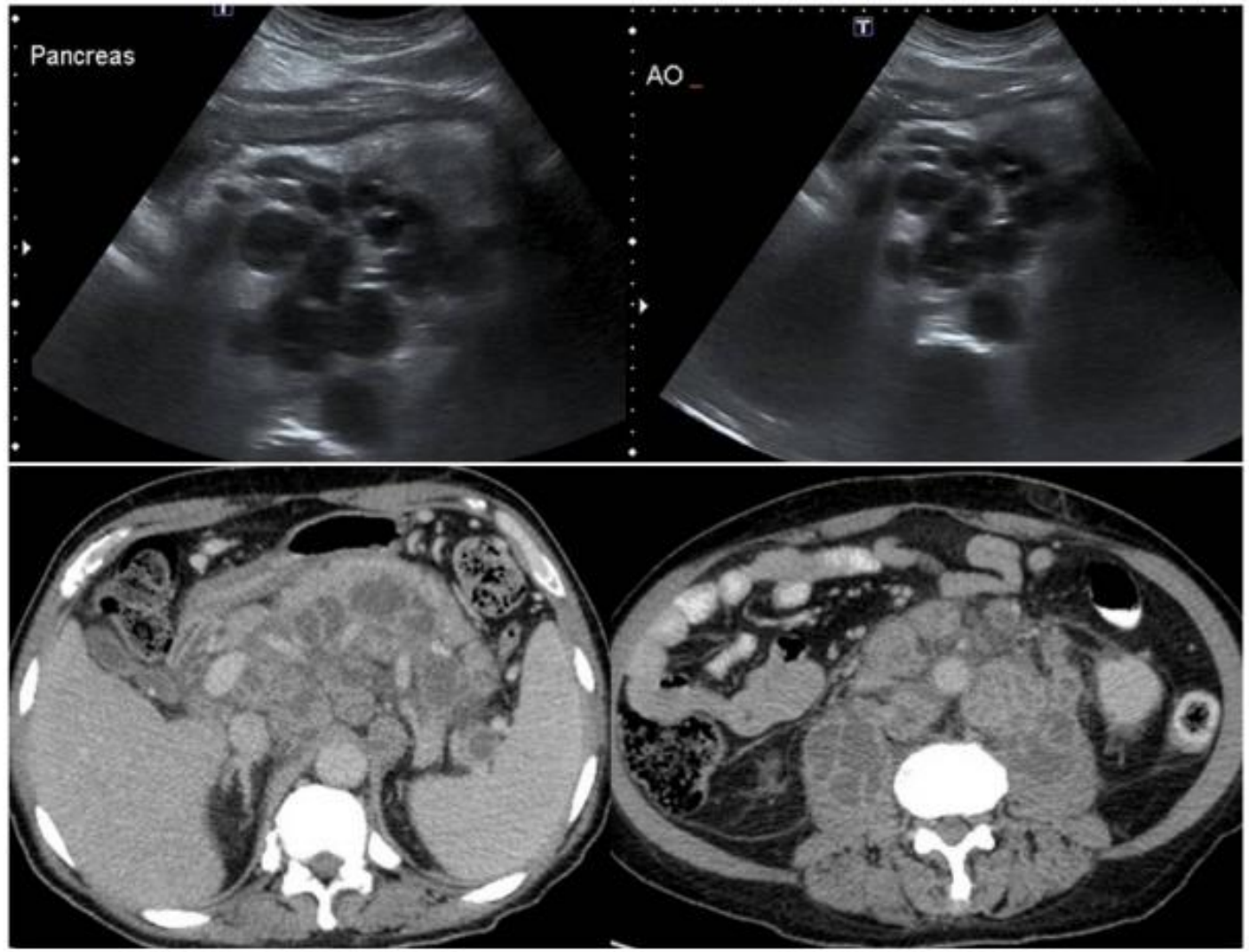

Figure 12. A 60 year-old man with AIDS and diffuse nodal TB. Abdominal ultrasound and CT demonstrate retroperitoneal bulky necrotic lymphadenopathy (arrows).

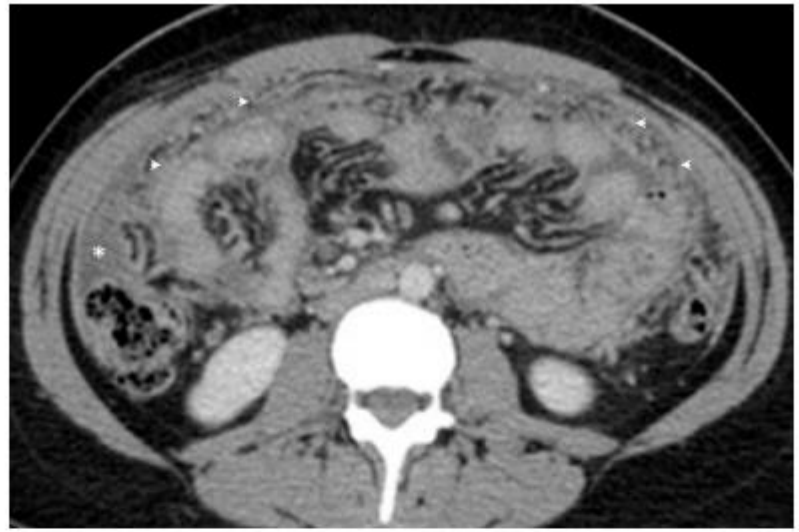

Figure 13. A 34 year-old female with Crohn's disease and disseminated active intra-thoracic and CNS tuberculosis. Contrast-enhanced CT abdomen shows mild ascites (asterisk), and diffuses peritoneal and omental thickening and nodularity (arrowheads). Biopsy of the omentum demonstrated granulomatous peritonitis.

Figure 14. A 40 year-old woman with active pulmonary and colonic TB. CT abdomen demonstrates marked circumferential wall thickening of the ascending colon (arrows).

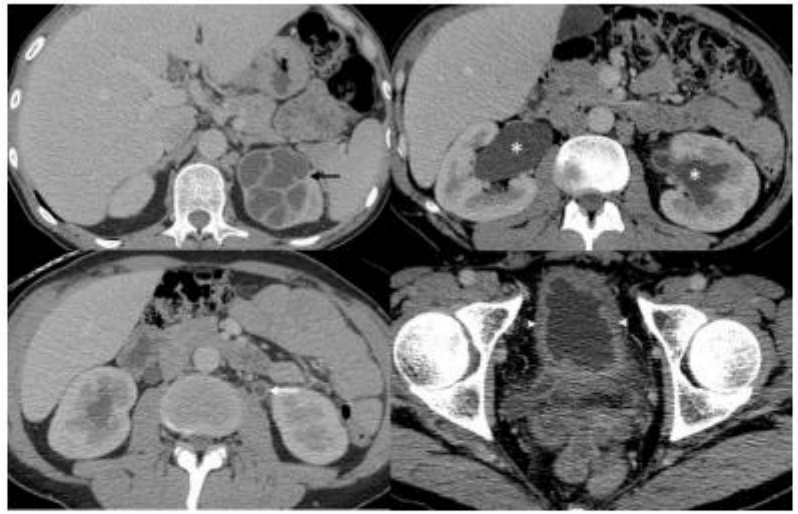

Figure 15. A 47 year-old man with active renal and bladder TB. CT abdomen shows bilateral hydronephrosis (asterisks), left upper renal pole caliectasis (black arrow), left ureter diffuse circumferential thickening and enhancement (white arrow), and diffuse wall thickening and trabeculations of the urinary bladder wall (arrowheads). Several retroperitoneal necrotic lymph nodes are also present.

Figure 16. A 70 year-old woman with remote pulmonary and left renal TB. CT abdomen shows left renal atrophy with peripheral coarse calcifications (arrows).

Figure 17. Cervical and dorsal tuberculous spondylodiscitis in a 41 year-old man with active pulmonary TB. Multisequential sagittal MRI of the dorsal spine demonstrates abnormal signal intensity and loss of T6-T7 disc space, opposing end plate irregularities, bone marrow enhancement of T6 and T7, and severe destruction of T7 vertebra. There is associated paravertebral collection (arrows) and small anterior intracanalicular epidural extension (arrowheads), compressing the spinal cord.

Figure 18. Tuberculous arthritis in a 42 year-old woman with active pulmonary TB. Top panel: multiplanar, multisequential MRI of the pelvis shows marked synovitis and effusion of the left hip joint, with associated bone marrow edema involving the acetabular and femoral sides. Bottom panel: three years later, radiograph and CT of the pelvis demonstrate left hip degenerative changes which required total hip joint replacement.

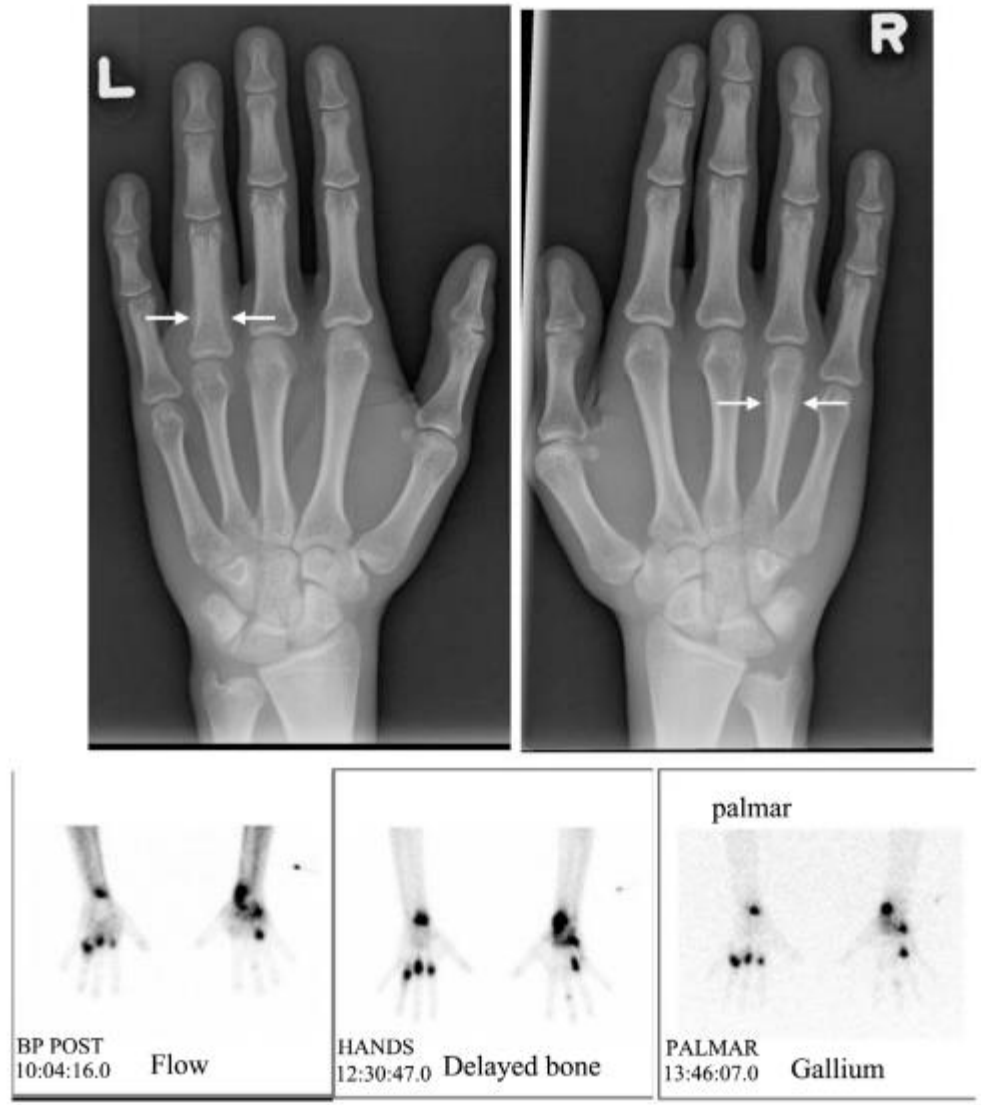

Figure 19. A 15 year-old man with active pulmonary TB and multifocal osteomyelitis. Radiographs of both hands show periosteal reaction around left 4th proximal phalanx and right 4th metacarpal. Bone scan shows hyperemia on flow study and increased activity on delayed images in right 4th MCP, wrist and distal right radius, left 2nd, 3rd and 4th MCP and distal left radius. The 48 hour gallium scan shows increased activity in the left 2nd, 3rd and 4th MCPs, in the right 4th MCP, in both distal radial metaphyses, and diffuse increased activity in the right wrist.

Ultrasound Evaluation and Guided Injection of the Subscapularis and Serratus Anterior Muscles Between the Scapula and the Thoracic Cage

A Technical Note

Daniel Chiung-Jui Su, MD, RMSK, CIPS, Chen-Yu Hung, MD, RMSK, King Hei Stanley Lam, MBBS, MScSEM, MScSMHS, RMSK, CIPS, FIPP, POCUS (MSK)

Video online at jultrasoundmed.org

Supplemental material online at jultrasoundmed.org

Received October 31, 2023, from the Department of Physical Medicine and Rehabilitation, Chi Mei Medical Center, Tainan, Taiwan (D.C.-J.S.); Department of Physical Medicine and Rehabilitation, National Taiwan University Hospital, Taipei, Taiwan (C.-Y.H.); The Department of Clinical Research, The Hong Kong Institute of Musculoskeletal Medicine, Kowloon, Hong Kong (K.H.S.L.); Faculty of Medicine, The

Most subscapularis and serratus anterior muscles lie between the scapula and the thoracic cage. Evaluation of this area in patients with scapulothoracic dyskinesis, snapping scapular syndrome, or interscapular pain can provide valuable information to clinicians. However, ultrasound scanning of pathologies in this area is hindered by anatomical limitations. In this study, we described a simple patient setup position and scanning method for ultrasound evaluation and guided intervention of the subscapularis and serratus anterior muscles between the scapula and thoracic cage.

Key Words—serratus anterior; sonoanatomy; subscapularis; ultrasound-guided injection; ventral scapula

Figure 1. A, The patient is in a side-lying position with the examined scapula against the bed. **B**, Depicted anatomy of the ventral s
the scapula (the rhomboids have been removed).

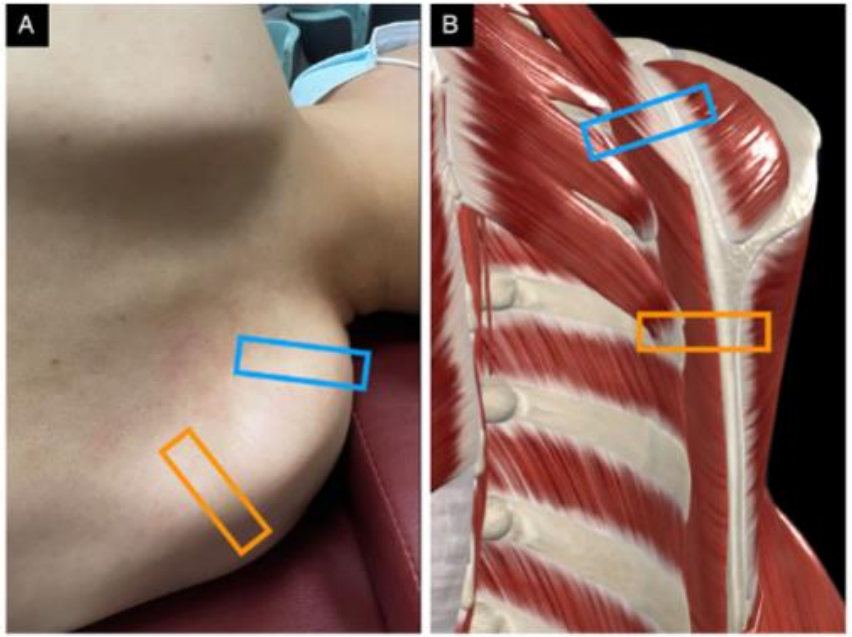

Figure 2. A and **B**, Sonoanatomy of the ventral surface of the scapula cephalic to the spine of the scapula (Probe position: Blue square in Figure 1). Yellow lines denote the borders of muscles and bone. The green circle is the spinal accessory nerve. The red circle is the dorsal scapular neurovascular bundles. SA, serratus anterior.

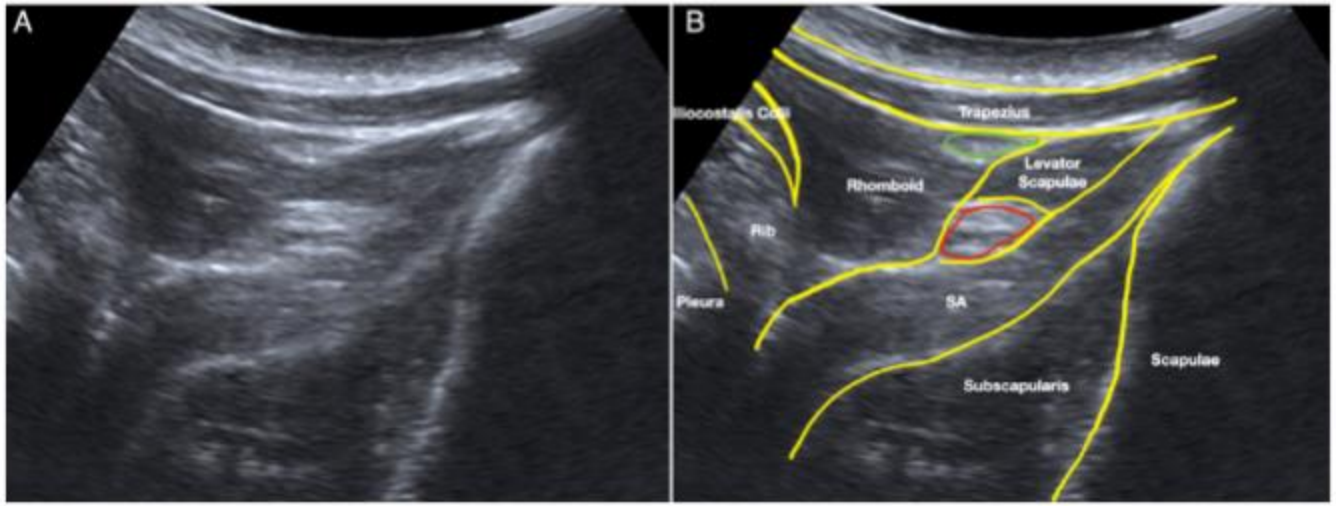

Figure 3. A and **B**, Sonoanatomy of the ventral surface of the scapula caudal to the spine of the scapula (Probe position: Orange square in Figure 1). Yellow lines denote the borders of muscles and bone. The red circle is the dorsal scapular neurovascular bundles. SA, serratus anterior.

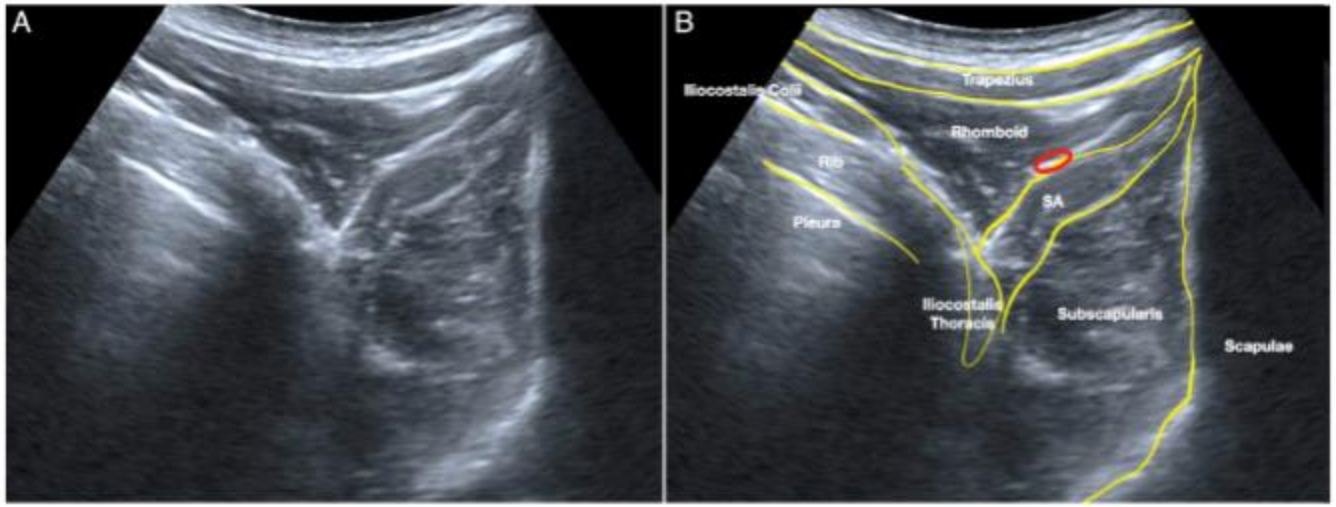

Figure 4. A and **B**, Comparison between healthy and chronic tears with fibrotic change (Yellow circle) over the subscapularis and serratus anterior muscle. SA, serratus anterior.

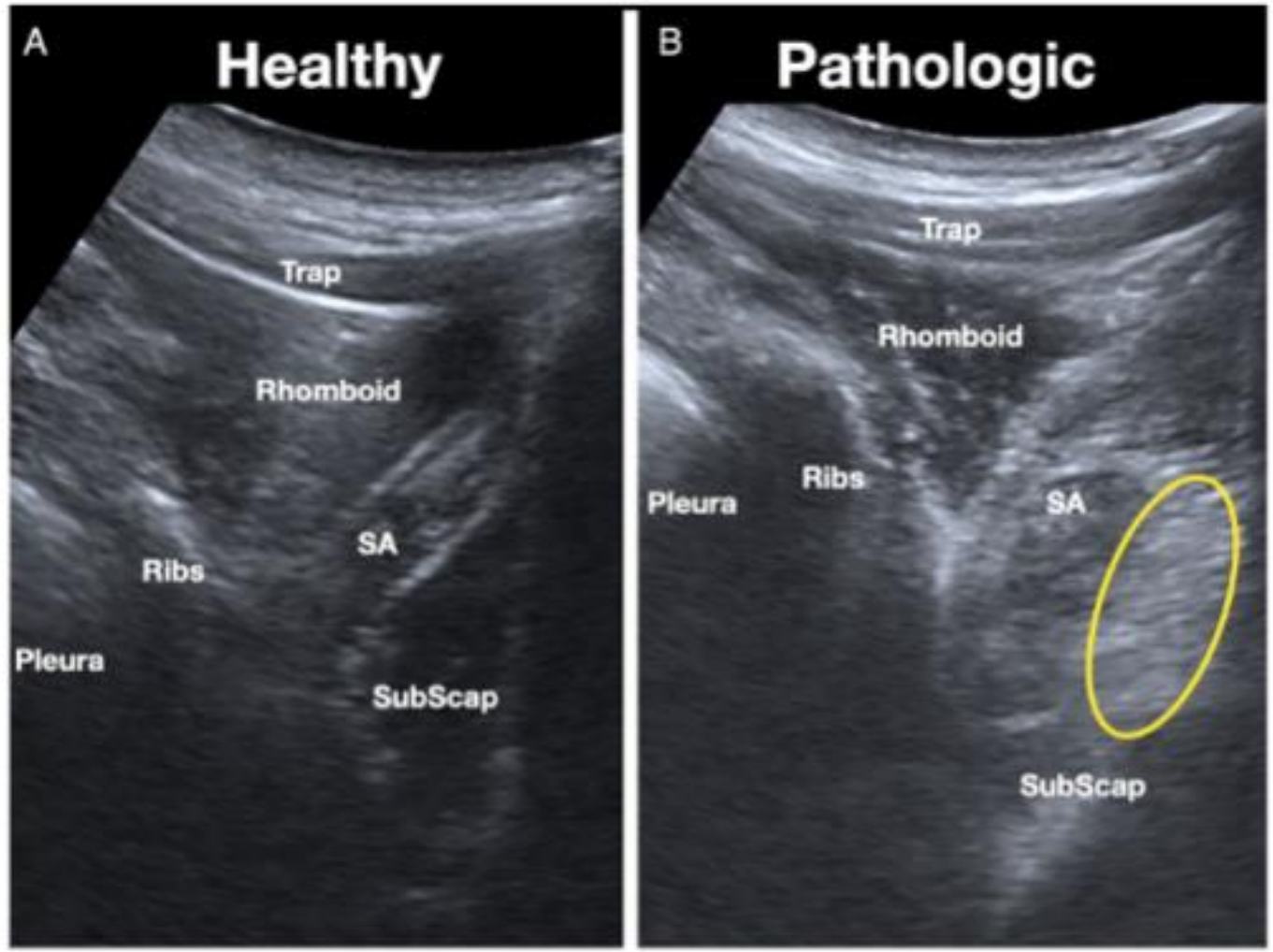

Median Nerve Shear Wave Elastography Is Associated With the Neurophysiological Severity of Carpal Tunnel Syndrome

Lauri Martikkala, MD, Antti Pemmari, MD, PhD, Sari-Leena Himanen, MD, PhD, Katri Mäkelä, MD, PhD

Received November 21, 2023, from the Faculty of Medicine and Health Technology, Tampere University, Tampere, Finland (L.M., A.P., S.-L.H.); and Department of Clinical Neurophysiology, Tampere University Hospital, Wellbeing Services County of Pirkanmaa, Tampere, Finland (A.P., S.-L.H., K.M.). Manuscript accepted for publication March 8, 2024.

This study was financially supported by Competitive State Research Financing of the Expert Responsibility area of Tampere University Hospital (Grants 9U007, 9V005, 9AB008).

None of the authors has any conflict of interest to disclose.

Address correspondence to Katri Mäkelä, Department of Clinical Neurophysiology, Tampere University Hospital, PO Box 2000, FI-33521 Tampere, Finland.

Objectives—This study examines the associations between the median nerve (MN) shear wave elastography (SWE), the MN cross-sectional area (CSA), patient's symptoms, and the neurophysiological severity of carpal tunnel syndrome (CTS). The most appropriate site to perform SWE was also tested.

Methods—This prospective study comprised 86 wrists of 47 consecutive patients who volunteered for MN ultrasound after an electrodiagnostic study. The neurophysiological severity of CTS was assessed according to the results of a nerve conduction study (NCS). The MN CSA was measured at the carpal tunnel inlet (wCSA) and the forearm (fCSA). SWE was performed on the MN in a longitudinal orientation at the wrist crease (wSWE), at the forearm (fSWE), and within the carpal tunnel (tSWE).

Results—The wCSA and wSWE correlated positively with the neurophysiological severity of CTS ($r = .619$, $P < .001$; $r = .582$, $P < .001$, respectively). The optimal cut-off values to discriminate the groups with normal NCS and with findings indicating CTS were 10.5 mm^2 for the wCSA and 4.12 m/s for the wSWE. With these cut-off values, wCSA had a sensitivity of 80% and specificity of 87% and wSWE a sensitivity of 88% and specificity of 76%. Neither tSWE nor fSWE correlated with the neurophysiological severity of CTS or differed between NCS negative and positive groups ($P = .429$, $P = .736$, respectively).

Conclusion—Shear wave velocity in the MN at the carpal tunnel inlet increases in CTS and correlates to the neurophysiological CTS severity equivalently to CSA measured at the same site.

Key Words—carpal tunnel syndrome; cross-sectional area; median nerve; shear wave elastography; ultrasound

Figure 1. The median nerve (MN) at the carpal tunnel inlet, marked with arrows. The top image demonstrates the cross-sectional area measurement (wCSA) and the second image the longitudinal view of the MN in B-mode. The bottom image demonstrates the SWE method. MN is visualized in longitudinal orientation in a dual image. On the left, the overlaid color map shows the reliable measurement index. The SWE stiffness map is shown on the right. Three region of interest points are inserted on the MN. In the wrist shown, there were no signs of CTS in the NCS.

Figure 6. SWE-stiffness map at the carpal tunnel intel site in a wrist with severe CTS indicating nerve conduction study findings in a 57-year-old man. The cross-sectional area of the median nerve at the carpal tunnel inlet was 17 mm^2. The motor distal latency was prolonged to 7.4 ms.

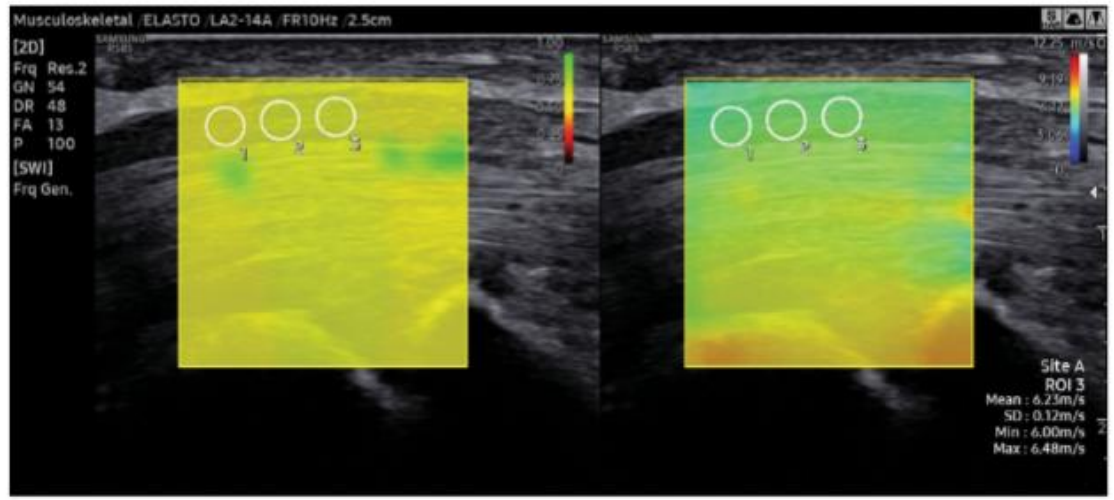

Figure 7. A, ROC curve of the wCSA and **B**, ROC curve of the wSWE to differentiate between the NCS-negative and NCS-positive groups.

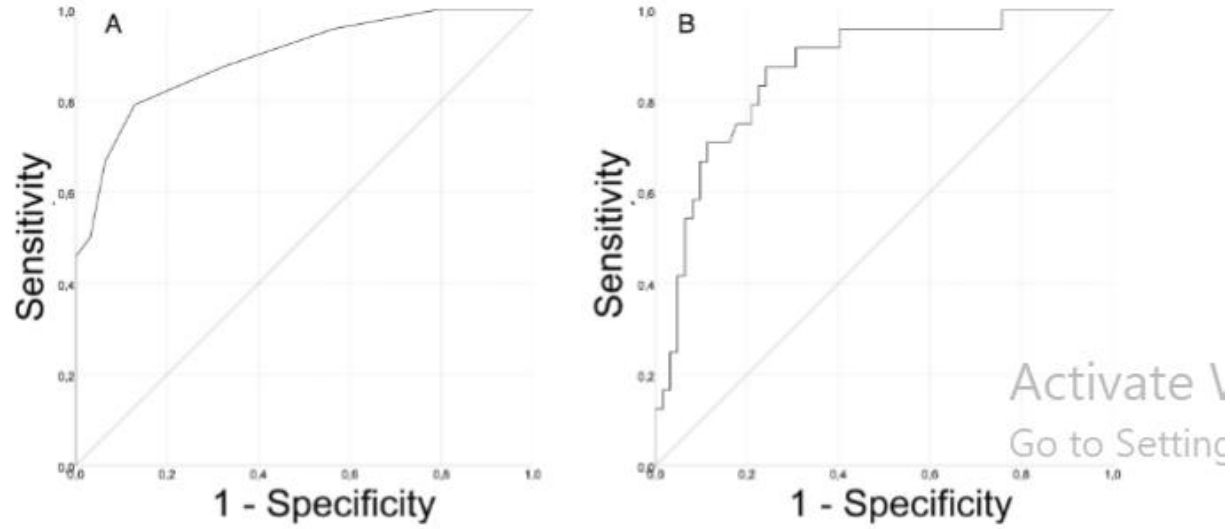

lnrads.com

+48 502-592-679 contact@lnrads.com

LN-RADS - Lymph Nodes Reporting and Data System

With the innovative LN-RADS approach, we are transforming the way lymph nodes are diagnosed. Using multiparametric, morphological criteria, we can detect very small macrometastes – even 2-3mm lesions. Compared to the traditional 10mm SAD size criteria, LN-RADS can find more than 20% of metastatic lymph nodes. Quick evaluations are ensured by the heuristic assessment model. The simplicity of LN-RADS allows for better communication between radiologists and clinicians. LN-RADS can be used in US, CT, MR and PET.

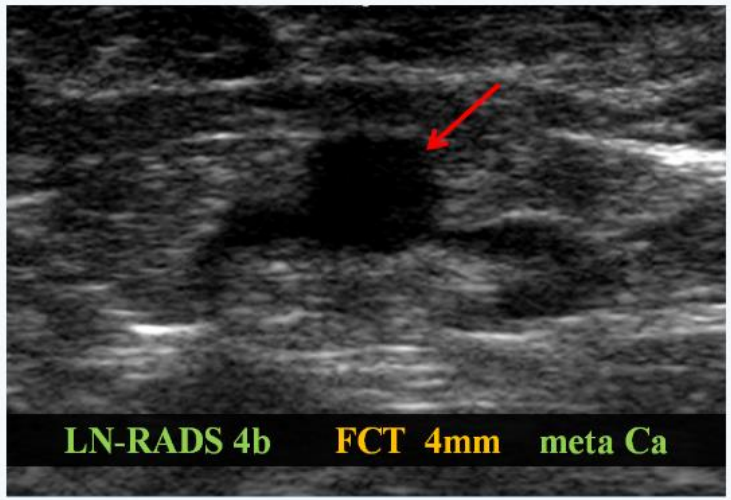

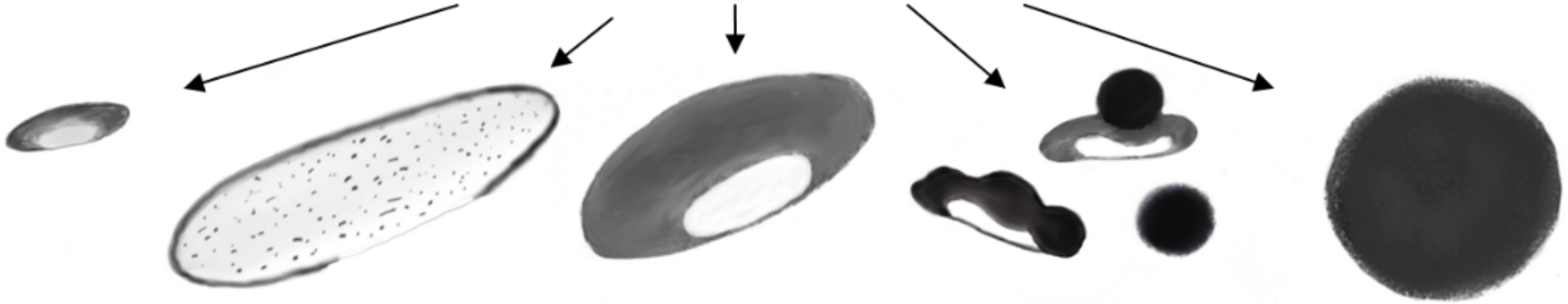

NORMAL	STEATOTIC	REACTIVE	SUSPICIOUS	MALIGNANT
Normal size, shape and structure*	Often enlarged cortex thin, regular hilum wide, fatty *	Usually enlarged regular thickenned cortex and preserved hilum*	MALIGNANCY SUSPICIOUS irregular cortex thickenning, FCT * low risk high risk	Enlargment and other malignance features*.

ONCO HISTORY

NO

YES

SYSTEMIC

estimated risk of malignancy

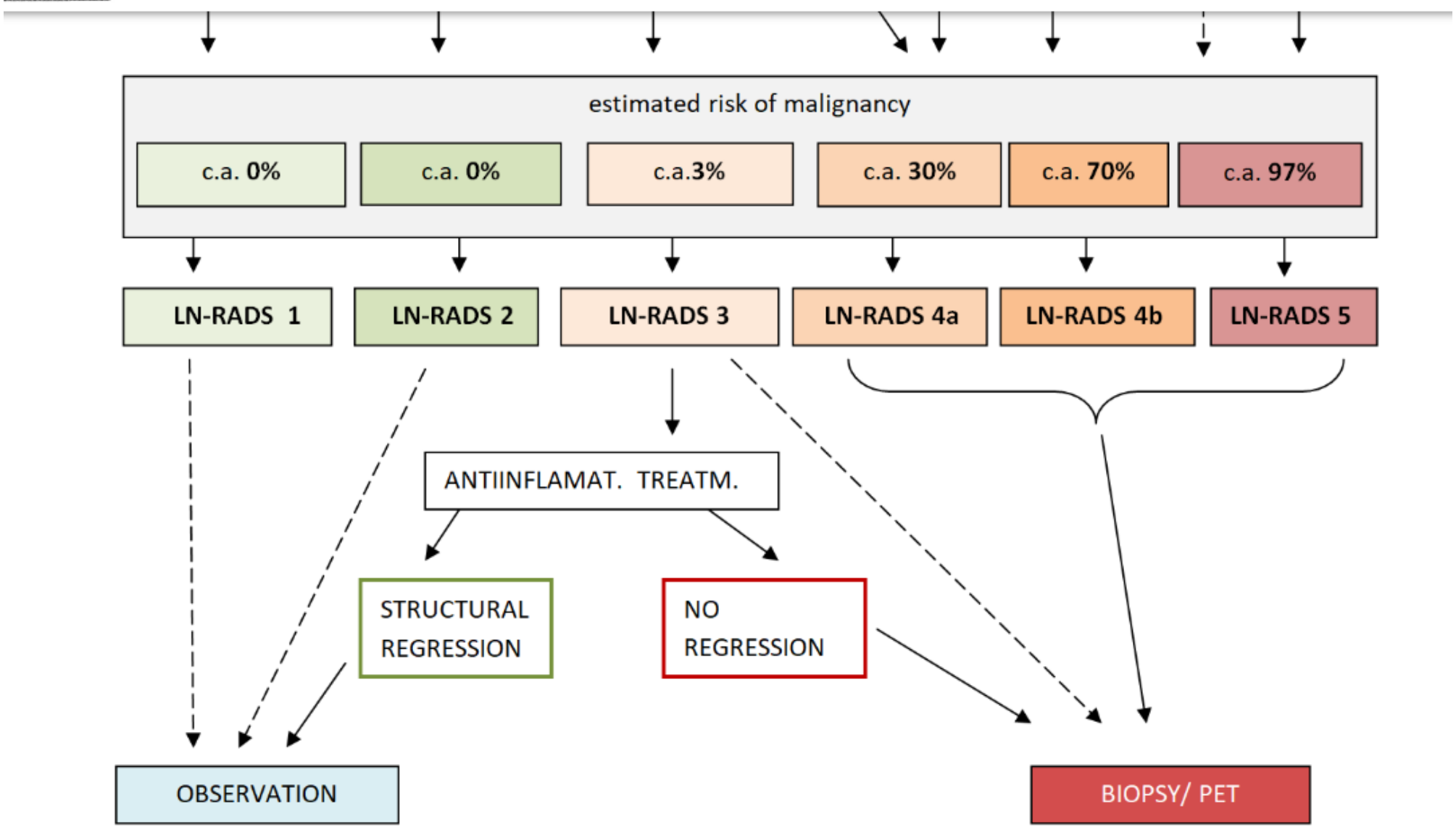

LN-RADS US criteria recommendation ver.1.0

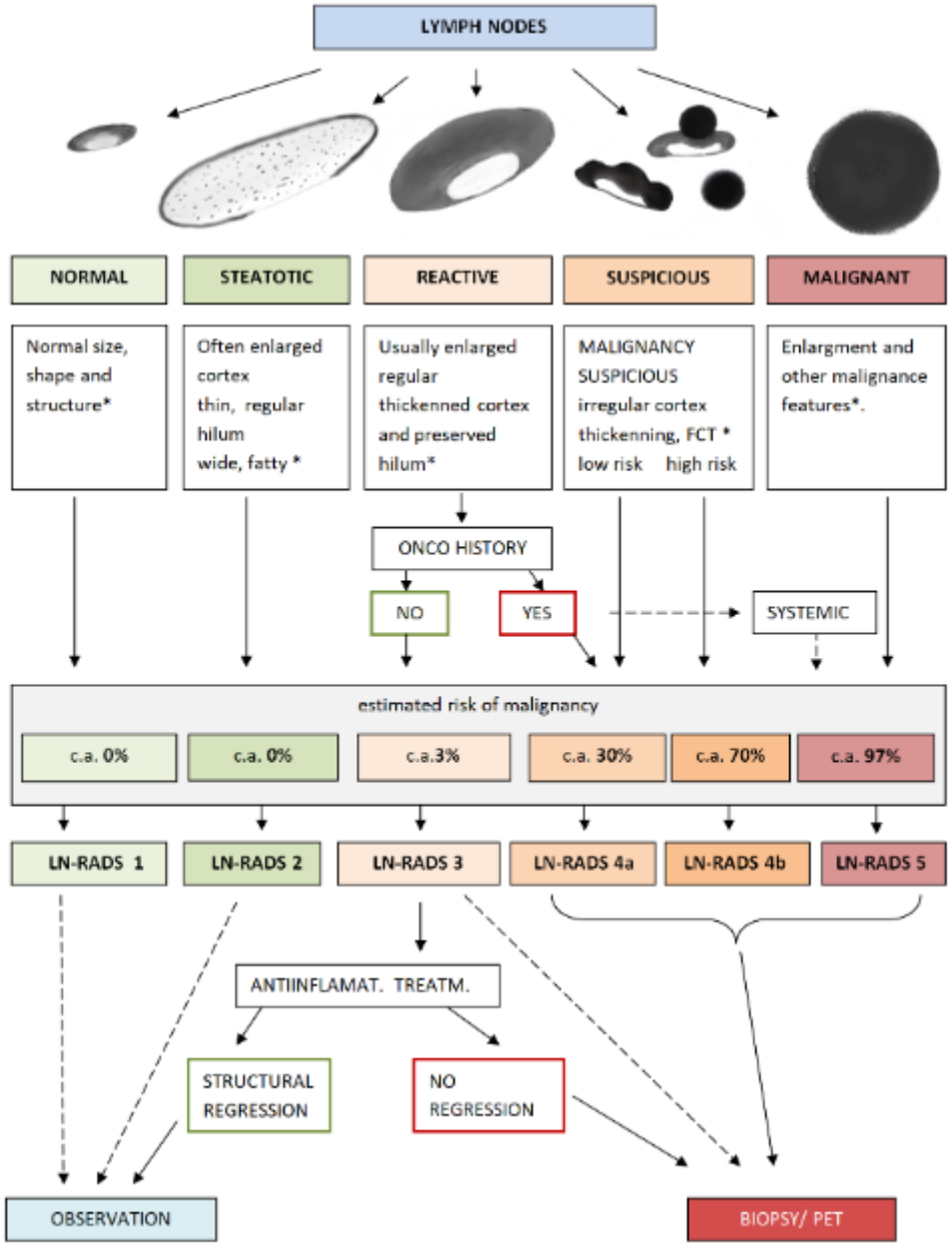

LN-RADS US criteria recommendation ver.1.0